View metadata, citation and similar papers at core.ac.uk

brought to you by CORE

provided by Warwick Research Archives Portal Repository

THE UNIVERSITY OF WARWICK

Original citation:
Marlow, Victoria A., Rea, Dean, Najmudin, Shabir, Wills, Martin and Fulop, Vilmos. (2013) Structure and mechanism of acetolactate decarboxylase. ACS Chemical Biology . ISSN 1554-8929

Permanent WRAP url:
http://wrap.warwick.ac.uk/56562

Copyright and reuse:
The Warwick Research Archive Portal (WRAP) makes this work of researchers of the University of Warwick available open access under the following conditions. Copyright © and all moral rights to the version of the paper presented here belong to the individual author(s) and/or other copyright owners. To the extent reasonable and practicable the material made available in WRAP has been checked for eligibility before being made available.

Copies of full items can be used for personal research or study, educational, or not-for-profit purposes without prior permission or charge. Provided that the authors, title and full bibliographic details are credited, a hyperlink and/or URL is given for the original metadata page and the content is not changed in any way.

Publisher's statement:
This document is the Accepted Manuscript version of a Published Work that appeared in final form in ACS Chemical Biology, copyright © American Chemical Society after peer review and technical editing by the publisher. To access the final edited and published work see http://dx.doi.org/10.1021/cb400429h

The version presented here may differ from the published version or, version of record, if you wish to cite this item you are advised to consult the publisher's version. Please see the 'permanent WRAP url' above for details on accessing the published version and note that access may require a subscription.

For more information, please contact the WRAP Team at: publications@warwick.ac.uk

warwickpublicationswrap

highlight your research

http://wrap.warwick.ac.uk/

Structure and mechanism of acetolactate decarboxylase

Victoria A. Marlow,[†,‡,§] Dean Rea,[‡] Shabir Najmudin,[‡] Martin Wills,[§] and Vilmos Fülöp[‡]*

[†]MOAC Doctoral Training Centre, The University of Warwick, Coventry, CV4 7AL, UK.

[‡]School of Life Sciences, The University of Warwick, Coventry, CV4 7AL, UK.

[§]Department of Chemistry, The University of Warwick, Coventry, CV4 7AL, UK.

KEYWORDS acetolactate decarboxylase, acetoin biosynthesis, stereoselective decarboxylation, bifunctional enzyme.

ABSTRACT: Acetolactate decarboxylase catalyzes the conversion of both enantiomers of acetolactate to the (*R*)-enantiomer of acetoin, via a mechanism that has been shown to involve a prior rearrangement of the non-natural *(R)*-enantiomer substrate to the natural (*S*)-enantiomer. In this paper, a series of crystal structures of ALDC complex with designed transition state mimics are reported. These structures, coupled with inhibition studies and site-directed mutagenesis provide an improved understanding of the molecular processes involved in the stereoselective decarboxylation/protonation events. A mechanism for the transformation of each enantiomer of acetolactate is proposed.

Acetolactate decarboxylase [EC 4.1.1.5] (ALDC) catalyzes the decarboxylation of (*S*)-α-acetolactate **1** (the natural substrate) and (*S*)- α-acetohydroxybutyrate **2** to (*R*)-acetoin **3** and (*R*)-3-hydroxypentan-2-one **4** respectively (Scheme 1).[1-11] As well as having significance in the brewing process,[5] ALDC has been used for the synthesis of enantiomerically-pure diols.[6] An interesting feature of this enzyme is that it also catalyses, at a lower rate, the decarboxylation of the corresponding (*R*)-enantiomer of **1** to give (*R*)-**3**, and also the conversion of (*R*)- α-acetohydroxybutyrate **2** to (*R*)-2-hydroxypentan-3-one **5** (Scheme 1).[7-11]

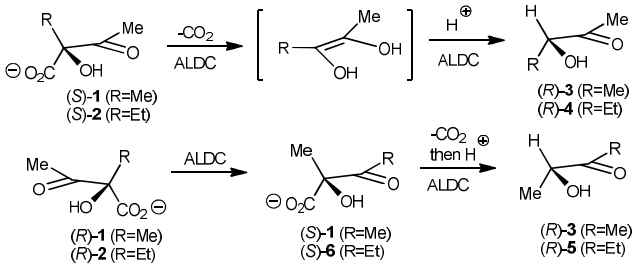

Scheme 1. Decarboxylation reactions catalyzed by ALDC.

Through a series of very careful ^{13}C-labelling and circular dichroism (CD) studies by Crout and coworkers[7-11] and Hill et al[4] (Supplementary Information), it was established that the high stereoselectivity of the reactions of (*S*)-**1** and (*S*)-**2** arises from decarboxylation to an intermediate enediol (or enolate) which is subsequently protonated on the face opposite that from which carbon dioxide was lost, and at the carbon atom to which it was attached, i.e. resulting in overall inversion (Scheme 1).[9,10] A similar stereoselective protonation of an enolate within a chiral enzyme environment following a decarboxylation has been reported in malonate decarboxylases.[12] The results observed for the (*R*)-enantiomers of ALDC substrates, in contrast, proceed via prior migration of the carboxylate group to the adjacent carbon atom via a conformation in which the C–O bonds are in a *syn* conformation.[7,8] From (*R*)-**1**, this results in the formation of a-acetolactate of (*S*)-configuration, i.e. the natural substrate, which subsequently undergoes decarboxylation to (*R*)-acetoin **3**. In the case of (*R*)-**2**, this rearrangement gives the structural isomer (*S*)-2-hydroxy-2-methyl-3-oxopentanoate, (*S*)-**6**, which then undergoes decarboxylation to the observed (*R*)-2-hydroxypentan-3-one (*R*)-**5**.[7] Hence ALDC appears to catalyze both the stereoselective decarboxylation/protonation and the rearrangement reaction of the non-natural substrate.

Due to a lack of X-ray crystallographic information on ALDC prior to our studies, less was known about the precise mechanism by which the enzyme directs the various reaction steps described above. Although during our analyses we became aware of a PDB deposition of 1xv2 (Midwest Center for Structural Genomics; www.mcsg.anl.gov): a crystal structure of a hypothetical protein similar to acetolactate decarboxylase from *Staphylococcus aureus*, since this was reported by a structural genomics consortium, no further analysis followed in the literature. In this paper, we describe the synthesis of a range of designed transition-state analogues and the X-ray crystal structures of their complexes with ALDC, together with results of inhibition and site-directed mutagenesis studies. These results identify the residues involved in the decarboxylation and rearrangement steps and provide the first molecular-level proposal for the catalytic mechanism of this functionally unique enzyme.

RESULTS AND DISCUSSION

Overall Structure. We have previously published the crystallization conditions and preliminary X-ray analysis of the

enzyme ALDC,[13] and have now completed the structure determination using the Single Wavelength Anomalous Dispersion (SAD) method at 1.1 Å resolution. ALDC is a metalloprotein with two domain α/β tertiary structure. The N-terminal domain comprises a 7 stranded mixed β-sheet that extends into the equivalent β-sheet of the 2-fold symmetry-related molecule generating a 14 stranded β-sheet that spans the physiologically relevant dimeric assembly (Figure 1A). Three highly conserved histidines (194, 196 and 207), coordinate a Zn^{2+} ion, together with a conserved glutamate (253) from the C-terminal tail. 3-Histidine-coordination of a metal ion has been reported in other enzymes including manganese in oxalate decarboxylase,[14] copper in quercetin 2,3-dioxygenase[15] and zinc in carbonic anhydrase (see Supporting Information).[16] Ethane-1,2-diol was used as a cryoprotectant, and was also observed to coordinate to the zinc ion through both oxygen atoms. There are three highly conserved residues (Thr58, Glu65 and Arg145) in the vicinity of the metal (Figure 1B). Unlike some other decarboxylase enzymes[17] ALDC does not contain a basic lysine residue capable of forming an imine intermediate prior to decarboxylation.

Figure 1

The coordination mode of ethane-1,2-diol suggested that acetolactate might bind to the zinc ion through the ketone and alcohol groups respectively since these are similarly spaced. If this is the case, then ALDC may promote decarboxylation through a mechanism in which the ketone and alcohol groups are chelated to the zinc ion (Figure 2A). This would restrict the C-O bonds in the required *syn* orientation[7-11] to assist decarboxylation and formation of an enol (or enolate) which is subsequently protonated in a stereoselective manner to furnish the observed product.

Figure 2

Transition State Analogues. In view of this proposed mechanism, we sought a suitable molecule to act as a mimic of the transition state, i.e. that would occupy a corresponding position in the active site for crystallographic and inhibition studies. In this respect, the diol of general structure **7** appeared to be an appropriate candidate. Diol **7** contains a carboxylate group to mimic the position of the ketone group of the substrate (Figure 2B), which gains an increasing negative charge as the decarboxylation proceeds. The mimic of the substrate carboxylic acid is provided by a hydroxy group, which contains appropriate functionality to act as both a hydrogen bond donor and acceptor to adjacent residues. Diol **7** can exist in four stereoisomeric forms. Of these, the inhibitors of (*R*) configuration at C2 would be expected to best mimic the natural substrates (Figure 2B). Following literature precedents,[18,19] we employed an asymmetric dihydroxylation reaction of the appropriate methyl angelate or tiglate ester, followed by ester hydrolysis, to prepare each of the four possible enantiomerically-enriched transition state analogue molecules **7** (Figure 2C); full details of the synthesis are given in the Supporting Information.

Kinetic Studies. Kinetic studies were conducted on ALDC from *Bacillus brevis* (provided by Novozymes) and *Bacillus subtilis* (33% sequence identity, cloned, expressed and purified in-house; Supporting Information). Kinetic data were determined using circular dichroism, the use of which has previously been reported as a convenient method for studies on ALDC.[10,20,21] Attempts to use a Voges-Proskauer assay or a coupled assay with generation of NAD^+ were less successful (Supporting Information). The CD assays required the use of enantiomerically-enriched substrate (*S*)-**1**, therefore a new synthetic approach to this molecule was developed through the use of an enzyme-catalyzed kinetic resolution of (*2S,3S*)-**7**, followed by oxidation (Supporting Information).[22] This permitted the conversion to chiral acetoin to be followed in real time, since both enzyme substrate and product give peaks in different positions in the spectra (Supporting Information). Control experiments were carried out to confirm that significant uncatalyzed decarboxylation did not take place at pH < 12.7,[7,9] and the CD experiments were conducted in buffer at pH 6. All four transition state analogues were tested as inhibitors of *B. brevis* ALDC and K_i (inhibition constant) for each inhibitor was determined by global curve fitting (Table 1). Whilst not particularly tight-binding, all four compounds exhibited distinct enzyme inhibition. (*2R,3S)*-**7** acted in a mixed fashion, and the other 3 compounds showed competitive inhibition (Supporting Information).

Table 1

Transition State Analogue Structures. The four transition state analogues of general structure **7** were co-crystallized in turn with ALDC (sample from *B. brevis* supplied by Novozymes Ltd). The structures with the (*R,R*), (*S,S*) and (*S,R*)- isomers bound in the active site were determined (Figures 3A-3C). In the first two structures, the Glu65, Arg145 and Glu253 residues contact the analogues through hydrogen bonds and the inhibitors adopt essentially identical conformations. For the (*R,R*) enantiomer, the OH is positioned on the opposite side relative to that in the (*S,S*) and (*S,R*) complexes, and is bound to the zinc ion. Glu65 and Arg145 also form stabilizing hydrogen bonds. An attempt to form a complex of the (*R,S*) isomer with ALDC resulted in isolation of a crystal containing the enantiomeric (*S,R*) isomer (present as a minor impurity). This may reflect substantially stronger binding of the (*S,R*) isomer over the (*R,S*) isomer.

Figure 3

In an attempt to obtain the structure of the holoenzyme without a bound ligand we replaced the cryoprotectant ethane-1,2-diol with glycerol, which also bound to the Zn(II) ion (Figure 3D). Two of the OH groups in glycerol were bound, with the remaining one bound to adjacent residues in the same manner as the (*S,S*) and (*S,R*) inhibitors. Further efforts were made to obtain the structure of the holoenzyme by using CryoOil (Supporting Information), which resulted in a bound phosphate ion (Figure 3E). For comparative purposes, the structure of ALDC bound to ethane-1,2-diol is also illustrated in Figure 3E.

Reaction Mechanism. The observation of the mode of binding of the (*R,R*)-**7** isomer supports the proposed decarboxylation mechanism for the natural (*S*) enantiomer, also involving transient binding of the departing CO_2 to the zinc (Figure 4A). The role of the Zn(II), as a Lewis acid, is best understood in terms of the reverse reaction of acetoin carboxylation. Arg145 is well positioned to assist delivery of the proton which creates the new chiral center. For the non-natural (*R*) enantiomer, the observation of binding by (*S,S*)-**7** and (*S,R*)-**7** suggest that the R-substrate can bind as shown in Figure 4B, with additional interactions preventing decarboxylation but promoting carboxylate rearrangement. Rotation of the rearranged substrate within the active site allows it to enter the decarboxylation manifold of (*S*)-**1**. This process agrees with the known base-promoted rearrangement mechanism and the observation of the conversion of (*R*)-**1** and (*R*)-**2** to (*R*)-**3** and (*R*)-**5** respectively (Scheme 1). The observation of racemisation via carboxylate transfer in basic solution suggests that this process is concerted, rather than via release and re-addition of carbon dioxide. It is believed that this is also the case for the reaction in the enzyme.

Figure 4

Sequence identity across ALDC from different bacteria provides further support for the proposed mechanism (Supporting Information). The *B. subtilis* gene *alsD*, encoding ALDC, was amplified from genomic DNA by PCR and ligated into an expression vector and several active site mutants were made using site-directed mutagenesis. Five of the mutants showed very little activity; E62Q, E62A, R142A, E251Q and E251A and the rates were too low to be accurately measured. Three of the mutants were active; T55S was approximately 2-fold more active, T55A was approximately 2.5-fold more active and R142K retained 40 % of the activity of native AlsD. The three active mutants were studied in more detail to measure kinetic parameters (Supporting Information). T55A and T55S have a similar K_M to native AlsD but have an increased k_{cat}, R142K has a decreased K_M and a decreased k_{cat}. The decreased K_M implies that the lysine mutant binds substrate with a greater affinity but is less effective as a catalyst and turns over substrate much slower. These results imply that both the glutamate residues are essential for catalysis. Lysine can partially compensate for the loss of the arginine residue implying that a basic residue is necessary for catalysis in this position. As the threonine mutants were more active than native AlsD it can be concluded that this residue is not involved in the catalytic mechanism of ALDC.

There is an analogy in the mechanism to that of fructose-1,6-bisphosphate aldolase[23] in which a similar zinc-bound 2-hydroxyenolate intermediate is formed. An additional contribution to reactivity could arise if the carboxylic acid groups were all present in the deprotonated carboxylate form. This would result in substrate destabilization by electrostatic repulsions between proximal carboxylate groups, as has been observed for related decarboxylation enzymes.[17,23,24]

In conclusion, we have used synthetic chemistry, crystallography and enzyme kinetic studies to propose a mechanism by which ALDC catalyzes both the decarboxylation of the favored S-acetolactate and the isomerization via carboxyl migration and subsequent decarboxylation of the less-favored R substrate.

METHODS

Crystallization of *B. brevis* ALDC. ALDC was supplied as a gift from Novozymes and stored at -80°C. For crystallization studies ALDC was concentrated to 13.5 mg/ml using a Vivaspin centrifugal concentrator with a molecular weight cut off of 10,000 Da. ALDC had previously been crystallized under three different conditions to give rise to 3 different crystal forms [25]. One of the conditions was further optimized to produce strongly diffracting crystals (1.1 Å resolution). The final conditions were: 0.2 M Trimethylamine N-oxide (TMAO), 0.1 M Tris pH 8.5, 28-33 % PEG 2K MME. Protein-ligand complex structures were obtained by growing crystals in the presence of 2,3-dihydroxy-2-methylbutanoic acid **7**. 1 M inhibitor was added to the protein in a 1:9 ratio. Crystals were cryoprotected either with 25 % glycerol or using LV CryoOil (MiTeGen) before they were transferred on a nylon loop directly into a 100K nitrogen cryostream.

Data Collection, Structure Determination and Refinement. Due to difficulty in at obtaining a suitable heavy atom derivative, a sulphur-SAD experiment was carried out on ALDC crystals at beam line BM14 at the ESRF, France. ALDC has 6 methionines out of 257 residues. Although it was not known at the time that ALDC contained a zinc ion, this atom also contributed significantly to the experimental phasing (Supporting Information). The resulting model was used to refine the high-resolution ligand bound structures. All X-ray data were collected at 100K. The ethane-1,2-diol bound data were collected at the beam line 9.6 the SRS, Daresbury, U.K. at wavelength of 0.8700 Å. The (*2R,3R*)-**7**, (*2S,3R*)-**7** and phosphate-bound data sets were obtained at beam line IO4 at the Diamond Light Source, U.K. using 0.9795 Å radiation. The (*2S,3S*)-**7** and glycerol bound data sets were collected using our in-house facilities using CuKα (1.5418 Å) radiation. All data were indexed, integrated and scaled using the XDS package.[25] Further data handling was carried out using the CCP4 software package.[26] The crystals belong to the trigonal space group $P3_221$ and contain one molecule per asymmetric unit with a solvent content of 46 % by volume. Refinement of the structure was carried out by alternate cycles of REFMAC[27] and manual refitting using O.[28] Water molecules were added to the atomic model automatically using ARP[29] at the positions of large positive peaks in the difference electron density, only at places where the resulting water molecule fell into an appropriate hydrogen bonding environment. Restrained isotropic temperature factor refinements were carried out for each individual atom. The polypeptide chain could be unambiguously traced in all structures between residues 20 and 255 or 256. Data collection and refinement statistics are given in Table 2.

Table 2

ASSOCIATED CONTENT

Supporting Information

Details of the synthetic chemistry (synthesis and characterization of all isomers of **7** and the enantiomerically-enriched acetolactate substrate), crystallographic structure determina-

tion, assay methods and the proposed mechanism of ALDC are given in Supporting Information. This material is available free of charge via the Internet at http://pubs.acs.org.

AUTHOR INFORMATION

Corresponding Author

*E-mail: V.fulop@warwick.ac.uk

Notes

The authors declare no competing financial interests.

Author Contributions

All authors have given approval to the final version of the manuscript.

ACKNOWLEDGEMENTS

We thank EPSRC for funding the MOAC doctoral training centre (VAM). We thank Jens T. Andersen, Shamkant A. Patkar and Torben V. Borchert (Novozymes) for a generous gift of ALDC derived from *B. brevis*. We are also indebted to Claire Dow for help with mutagenesis, David Porter for providing *B. brevis* genomic DNA, Alison Rodger for help and advice with CD studies and David Crout for useful discussions. Crystallographic data were collected at beam lines BM14 at ESRF, France, 9.6 at SRS, Daresbury and IO4 at Diamond Light Source, UK and we acknowledge the support of the beam line scientists. Some equipment used in this research was obtained through the Birmingham–Warwick Science City Translational Medicine: Experimental Medicine Network of Excellence project, with support from Advantage West Midlands (AWM).

REFERENCES

(1) Dolin, M. I. and Gunsalus, I. C. (1951) Pyruvic acid metabolism II.: An acetoin-forming enzyme system in Streptococcus faecalis. *J. Bacteriol. 62*, 199-214.

(2) Løken, J. P.and Størmer, F. C. (1970) Acetolactate decarboxylase from aerobacter-aerogenes - purification and properties. *Eur. J. Biochem. 14*, 133-137.

(3) Størmer, F. C. (1967) Isolation of Crystalline pH 6 Acetolactate-forming enzyme from *Aerobacter aerogenes. J. Biol. Chem. 242*, 1756-1759.

(4) Hill, R. K., Sawada, S. and Arfin, S. M. (1979) Stereochemistry of valine and isoleucine biosynthesis: IV. Synthesis, configuration, and enzymatic specificity of [α]-acetolactate and [α]-aceto-[α]-hydroxybutyrate. *Bioorg. Chem. 8*, 175-89.

(5) Dulieu, C., Moll, M., Boudrant, J. and Poncelet. D (2000) Improved performances and control of beer fermentation using encapsulated □-acetolactate decarboxylase and modeling. *Biotechnology progress 16*, 958–956.

(6) Yan, Y., Lee, C.-C. and Liao, J. C. (2009) Enantioselective synthesis of pure (*R,R*)-2,3-butanediol in *Escherichia coli* with stereospecific secondary alcohol dehydrogenases. *Org. Biomol. Chem. 7*, 3914-3917.

(7) Crout, D. H. G. and Rathbone, D. L. (1988) Biotransformations with acetolactate decarboxylase: Unusual conversions of both substrate enantiomers into products of high optical purity. *J. Chem. Soc. Chem. Commun*. 98-99.

(8) Crout, D. H. G. and Hedgecock, C. J. R. (1979) The base-catalysed rearrangement of α-acetolactate (2-hydroxy-2-methyl-3-oxobutanoate): a novel carboxylate ion migration in a tertiary ketol rearrangement. *J. Chem. Soc. Perkin Trans. 1*, 1982-1989.

(9) Crout, D. H. G., Littlechild, J., Mitchell, M. B. and Morrey, S. M. (1984) Stereochemistry of the decarboxylation of α-acetolactate (2-hydroxy-2-methyl-3-oxobutanoate) by the acetolactate decarboxylase of *Klebsiella Aerogenes*. *J. Chem. Soc. Perkin Trans. 1*, 2271-2276.

(10) Drake, A. F., Siligardi, G., Crout, D. H.G. and Rathbone, D. L. (1987) Applications of vibrational infrared circular-dichroism to biological problems - stereochemistry of proton-exchange in acetoin (3-hydroxybutan-2-one) catalyzed by acetolactate decarboxylase. *J. Chem. Soc. Chem. Commun*. 1834-1835.

(11) Crout, D. H. G., Lee, E. R. and Rathbone, D. L. (1990) Absolute configuration of the product of the acetolactate synthase reaction by a novel method of analysis using acetolactate decarboxylase. *J. Chem. Soc. Perkin Trans. 1*, 1367-1369.

(12) Okrasa, K., Levy, C., Wilding, M., Goodall, M., Baudeldistel, N., Hauer, B., Leys, D. and Micklefield, J. (2009) Structure-guided directed evolution of alkenyl and arylmalonate decarboxylases. *Angew. Chem. Int. Ed. 48*, 7691-7694.

(13) Najmudin, S., Andersen, J. T., Patkar, S. A., Borchert, T. V., Crout, D. H. G. and Fülöp, V. (2003) Purification, crystallization and preliminary X-ray crystallographic studies on acetolactate decarboxylase. *Acta Crystallogr. D. 59*, 1073–1075.

(14) Anand, R., Dorrestein, P. C., Kinsland, C., Begley, T. P. and Easlck, S. E. (2002) Structure of oxalate decarboxylase from *Bacillus subtilis* at 1.75 Å resolution. *Biochemistry 41*, 7659-7669.

(15) Fusetti, F., Schröter, K. H., Steiner, R. A., Van Noort, P.I., Pijning, T., Rozeboom, H. J., Kalk, K. H., Egmond, M. R. and Dijkstra, B. W. (2002) Crystal structure of the copper-containing quercetin 2,3-dioxygenase from *Aspergillus japonicas. Structure 10*, 259-268.

(16) Fisher, Z., Hernandez Prada, J. A., Tu, C., Duda, D., Yoshioka, C., An, H., Govindasamy, L., Silverman, D. N. and McKenna, R. (2005) Structure and kinetic characterisation of active-site histidine as a proton shuttle in catalysis by human carbonic anhydrase II. *Biochemistry 44*, 1097-1105.

(17) Ho, M.-C., Ménétret, J.-F., Tsuruta, H. and Allen, K. N. (2009) The origin of the electrostatic perturbation in acetoacetate decarboxylase. *Nature 459*, 393-397. Highlighted by Gerlt, J. A. (2009) Acetoacetate decarboxylase: hydrophobics, not electrostatics. *Nat. Chem. Biol. 5*, 454-455.

(18) Stritzke, K. Schulz, S. and Nishida, R. (2002) Absolute configuration and synthesis of β- and δ-lactones present

in the pheromone system of the giant white butterfly. *Idea Leuconoe*. *Eur. J. Org. Chem*. 3884–3892.

(19) Robins, D. J. and Crout. D. H. G. (1970) Pyrrolizidine alkaloids. The absolute configuration at C-2 in monocrotalic acid. *J. Chem. Soc. C: Organic 9*, 1334–1336.

(20) Vinogradov, M., Kaplun, A., Vyazmensky, M., Engel, S., Golbik, R., Tittmann, K., Uhlemann, K., Meshalkina, L., Barak, Z., Hubner, G. and Chipman, D. M. (2005) Monitoring the acetohydroxy acid synthase reaction and related carboligations by circular dichroism spectroscopy. *Anal. Biochem. 342*, 126-133.

(21) Crout, D. H. G. and Morrey, S. M. (1983) Synthesis *of R*- and *S*-acetoin. *J. Chem. Soc. Perkin Trans. 1*, 2435-2440.

(22) Moen, A. R., Ruud, K. and Anthonsen. T. (2008) Combination of stereospecific dihydroxylation and enzyme catalyzed enantioselective resolution for synthesis of enantiopure vicinal diols. *J. Mol. Catal. B: Enzymatic 50*, 74–79.

(23) Hall, D. R., Leonard, G. A., Reid, C. D., Watt, C. I. Berry, A. and Hunter, W. N. (1999) The crystal structure of *Escherichia Coli* class II fructose-1,6-bisphosphate aldolase in complex with phosphoglycolohydroxamate reveals details of mechanism and specificity. *J. Mol. Biol. 287*, 383-394.

(24) Chan, K. K., Wood, B. M., Federov, A. A., Federov, E. V., Imker, H. J., Amyes, T. L., Richard, J. P., Almo, S. C. and Gerit, J. A. (2009) Mechanism of the orotidine 5'-monophosphate decarboxylase-catalyzed reaction: Evidence for substrate destabilisation. *Biochemistry 48*, 5518-5531.

(25) Kabsch, W. (2010). XDS. *Acta crystallogr. D Biological crystallogr. 66*, 125-132.

(26) Collaborative Computational Project Number 4 (1994) The CCP4 suite: programs for protein crystallography. *Acta Crystallogr. D 50***,** 760-763.

(27) Murshudov, G.N., Vagin, A.A. and Dodson, E.J. (1997) Refinement of macromolecular structures by the maximum-likelihood method. *Acta Crystallogr. D 53*, 240-255.

(28) Jones, T.A., Zou, J.Y., Cowan, S.W. and Kjeldgaard, M. (1991) Improved methods for building protein models in electron density maps and the location of errors in these models. *Acta Crystallogr. A* 47, 110-119.

(29) Perrakis, A., Morris, R. and Lamzin, V.S. (1999) Automated protein model building combined with iterative structure refinement. *Nat. Struct. Biol. 6*, 458-463.

(30) Read, R.J. (1986) Improved Fourier coefficients for maps using phases from partial structures with errors. *Acta Crystallog A 42*, 140-149.

(31) DeLano, W. L. (2002). The PyMOL User's Manual, DeLano Scientific, Palo Alto, CA.

Table 1. Inhibition parameters for *B. Brevis* ALDC

Inhibitor	Mode of inhibition	V_{max} (mol min-1 mg-1)	K_M (mM)	K_i (mM)	R^2
(*2S,3S*)-**7**	Competitive	2269 ± 177	0.49 ± 0.14	0.46 ± 0.18	0.97
(*2R,3R*)-**7**	Competitive	2440 ± 247	0.55 ± 0.26	0.76 ± 0.40	0.94
(*2S,3R*)-**7**	Competitive	2216 ± 209	0.56 ± 0.28	1.72 ± 0.98	0.92
(*2R,3S*)-**7**	Mixed	2482 ± 320	0.78 ± 0.43	7.68 ± 8.89	0.88

Supplementary Table 1. Data Collection and Refinement Statistics of ALDC Bound Ligands[a]

	(*2R,3R*)-**7**	(*2S,3S*)-**7**	(*2S,3R*)-**7**	Glycerol	Phosphate	Ethane-1,2-diol
Data collection						
Space group	$P3_221$	$P3_221$	$P3_221$	$P3_221$	$P3_221$	$P3_221$
Cell dimensions						
a, *b*, *c* (Å)	47.11, 47.11, 198.91	47.14, 47.14, 198.66	46.83, 46.83, 198.28	47.13, 47.13, 198.89	47.01, 47.01, 198.97	46.95, 46.95, 198.90
α, β, γ (°)	90, 90, 120	90, 90, 120	90, 90, 120	90, 90, 120	90, 90 120	90, 90, 120
Resolution (Å)	35-1.1 (1.16-1.1)	41-1.6 (1.69-1.6)	35-1.1 (1.16-1.1)	41-1.6 (1.69-1.6)	32-1.1 (1.16-1.1)	41-1.1 (1.16-1.1)*
R_{sym} or R_{merge}	0.128 (0.761)	0.193 (0.837)	0.098 (0.797)	0.183 (1.010)	0.069 (0.345)	0.108 (0.234)
$I / \sigma I$	10.8 (2.4)	19.5 (4.6)	11.0 (2.0)	14.5 (3.4)	11.0 (3.3)	18.2 (3.6)
Completeness (%)	99.8 (99.4)	99.3 (97.4)	99.3 (95.1)	99.1 (94.1)	99.6 (99.8)	96.0 (80.2)
Redundancy	5.0 (3.6)	20.1 (18.7)	6.8 (5.1)	13.9 (12.2)	6.2 (6.2)	8.4 (3.3)
Refinement						
Resolution (Å)	35-1.1	41-1.6	35-1.1	41-1.6	32-1.1	41-1.1
No. reflections	105260	34150	104653	34655	104587	100592
R_{work} / R_{free}	0.207 / 0.225	0.180 / 0.210	0.177 / 0.184	0.171 /0.212	0.164 / 0.180	0.189 / 0.208
No. atoms						
Protein	1879	1879	1879	1890	1879	1890
Ligand/ion	10	10	10	25	6	5
Water	384	340	411	328	422	324
B-factors						
Protein	9.5	9.7	11.3	10.8	11.3	12.2
Ligand/ion	5.4	3.1	9.7	20.6	11.6	10.2
Water	13.8	14.4	18.3	20.6	20.1	20.6
R.m.s. deviations						
Bond lengths (Å)	0.015	0.016	0.016	0.016	0.015	0.014
Bond angles (°)	1.6	1.5	1.5	1.6	1.6	1.6
PDB ID	4BT3	4BT4	4BT5	4BT6	4BT7	4BT2

[a]Values in parentheses are for highest-resolution shell.

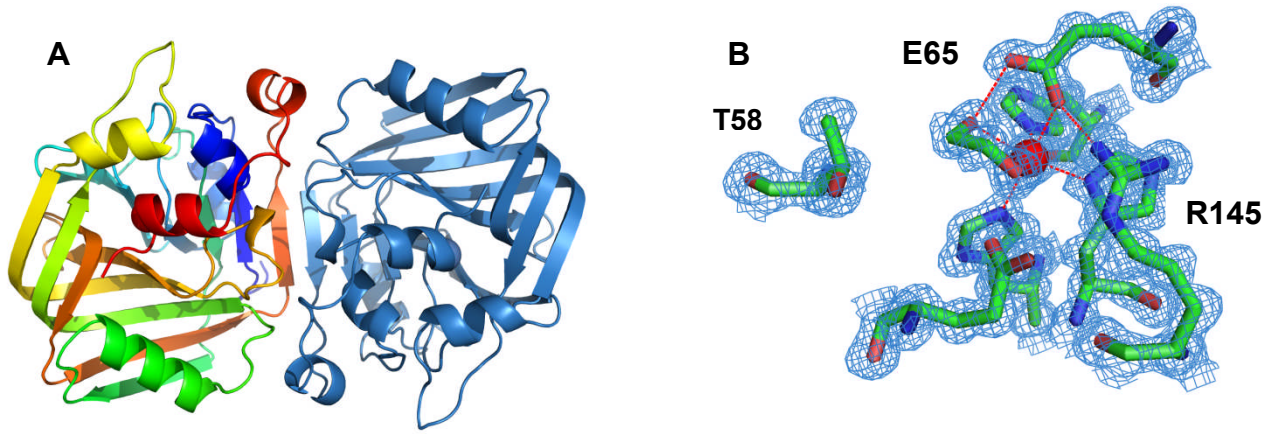

Figure 1. Crystallographic structure of ALDC from *Bacillus brevis*. (A) The tertiary and quaternary structure of ALDC. (B) ALDC bound to ethane-1,2-diol (Stereo view is in Supplementary Information, Figure S15).

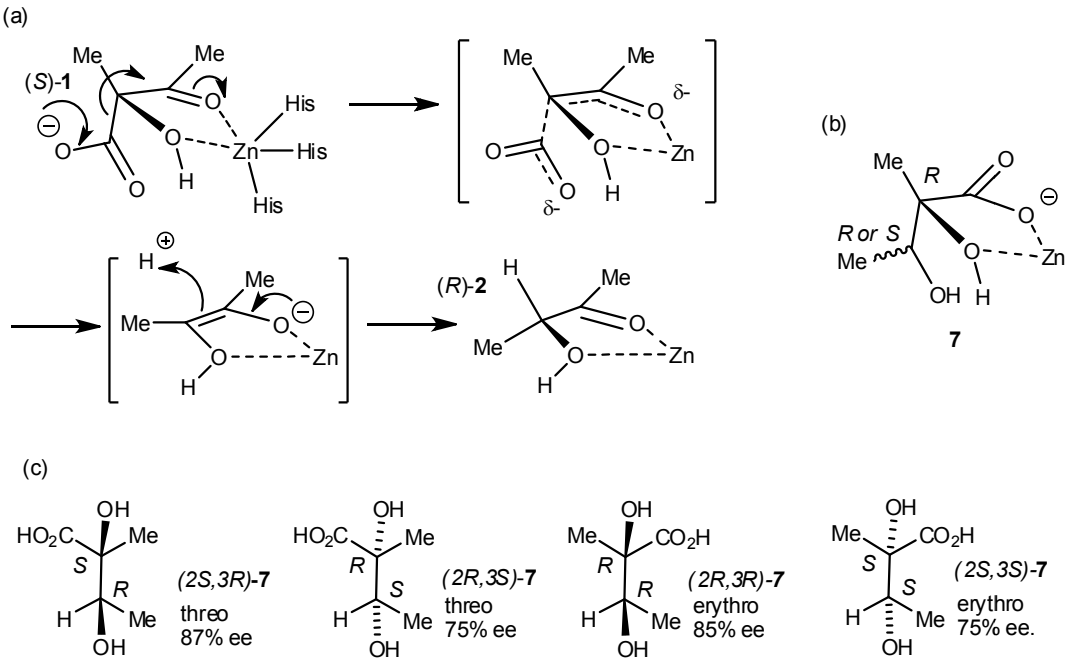

Figure 2. Reactions catalyzed by ALDC and transition state mimic. (A) Proposed decarboxylation reactions catalyzed by ALDC. (B) Proposed fit of (2*R*)-transition state mimics in the active site. (C) Transition-state mimics tested in this project.

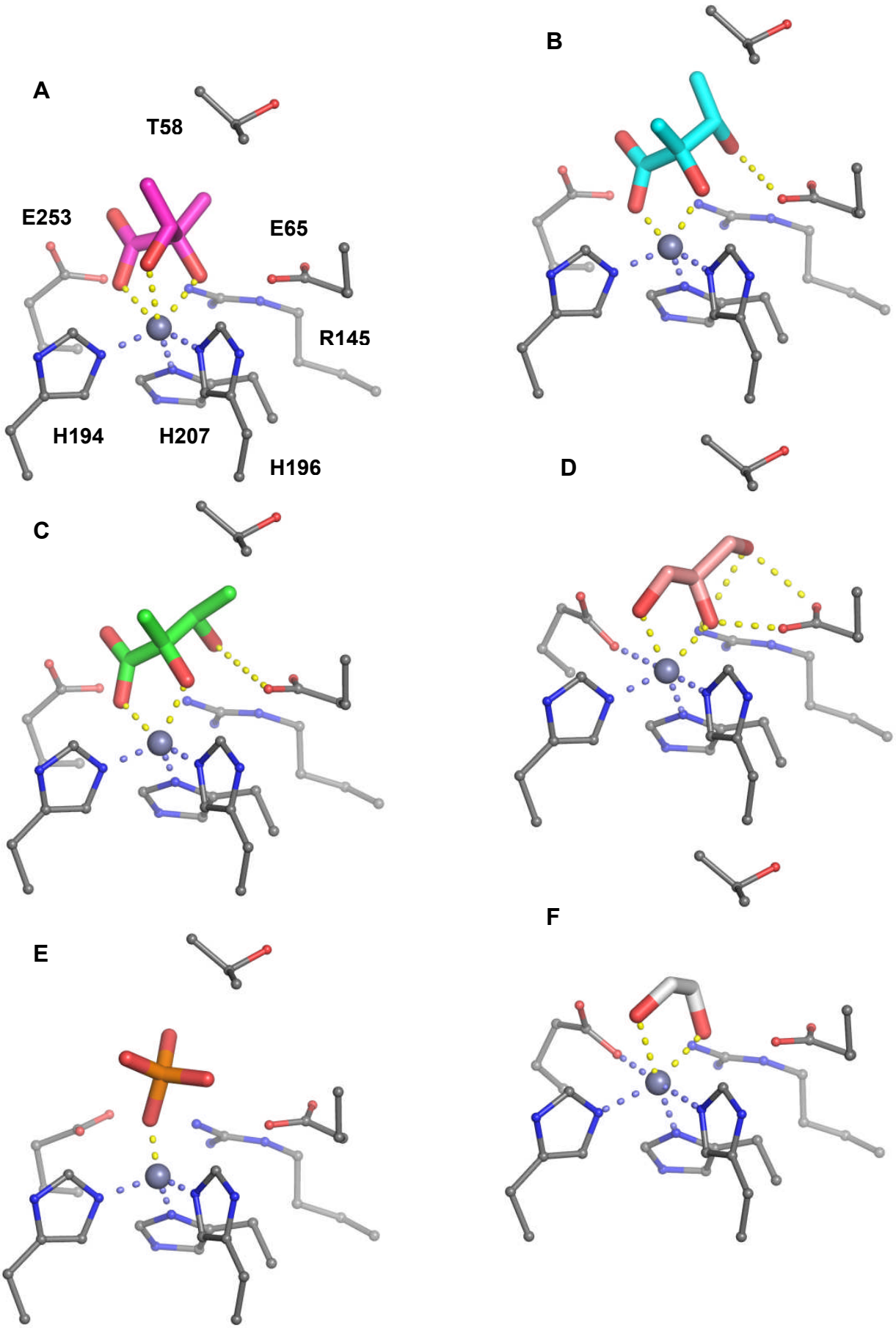
A
T58
E253
E65
R145
H194
H207
H196
B
C
D
E
F

Figure 3. ALDC structures with transition state analogues bound in the active site. (A) (*2R,3R*)-**7**, (B) (*2S,3S*)-**7**, (C) (*2S,3R*)-**7**, (D) Glycerol, (E) Phosphate, (F) Ethane-1,2-diol.

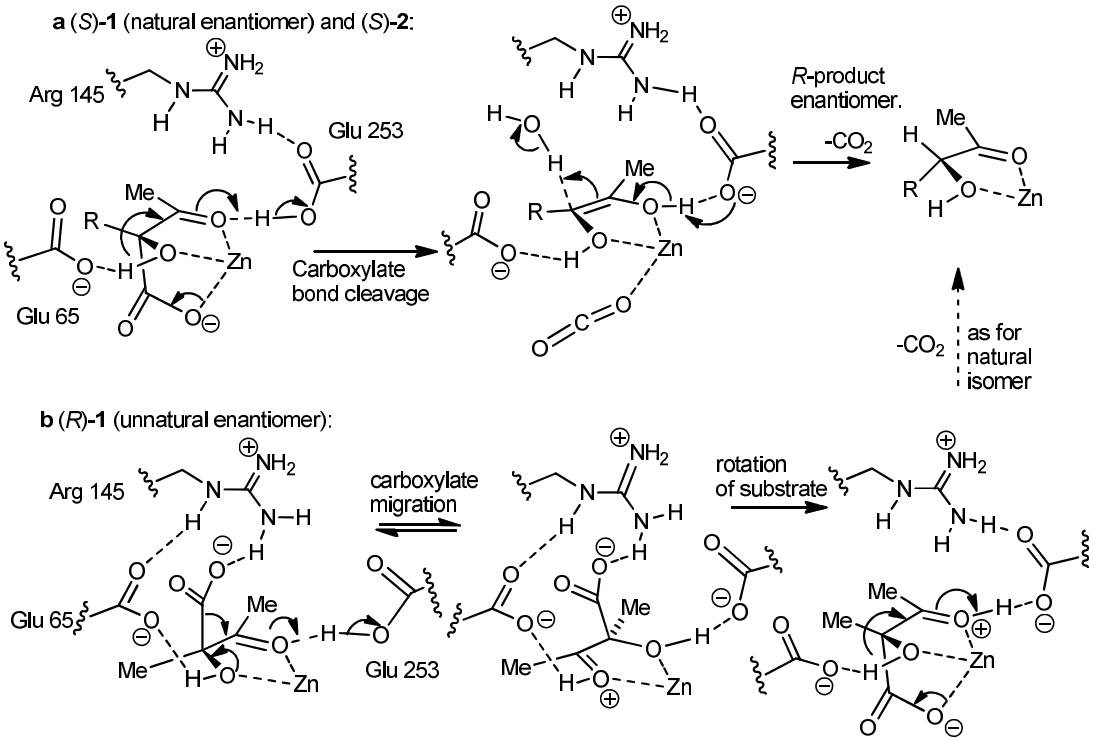

Figure 4. Proposed decarboxylation mechanism. (a) Proposed decarboxylation mechanism of (*S*)-**1** and (*S*)-**2** by ALDC, featuring a directed protonation (for (*S*)-**1**, R=Me, for (*S*)-**2**, R=Et). (b) Proposed decarboxylation of (*R*)-**1**- by ALDC, featuring a carboxylate migration and rearrangement prior to decarboxylation through the same mechanism as for the (*S*)- substrates. This results in formation of the (*R*)- **3** and product (*R*)-**5** containing transposed Me and Et groups.